Generalized two-field α-atractor models and hyperbolic surfaces

Mirela E. Babalic (with C.I. Lazaroiu and C.S. Shahbazi)

National Institute for Physics and Nuclear Engineering (NIPNE), Bucharest

SEENET-MTP Workshop BW2018
“Field Theory and the Early Universe”

June 10-14, 2018, Nis

Outline

1. Motivation
2. Two-field α-attractor models
3. Uniformization of hyperbolic surfaces
4. Inflation near the ends
5. Some examples
6. Conclusions

- Inflation in the early universe can be described reasonably well by the so-called two-field α-attractor models proposed by Linde, and which have as scalar manifold the Poincaré disk.
- We propose a wide generalization of these models, in the sense that:
  - we accept as scalar manifold (target space for the real scalar fields of the model) any hyperbolic surface which is geometrically finite and non-compact
  - we propose a general procedure for studying such models through uniformization techniques and without using one-field truncations.

Introduction

- In the standard cosmological framework, the early universe starts with a period of very fast exponential expansion called **inflation** (which explains the homogeneity and isotropy observed today) and finally it arrives to the present slowly accelerating universe.
- Inflationary models assume that the accelerated expansion of the universe is due to one or more scalar fields called **inflatons** whose potential energy dominates the energy density of the Universe during the inflationary period.

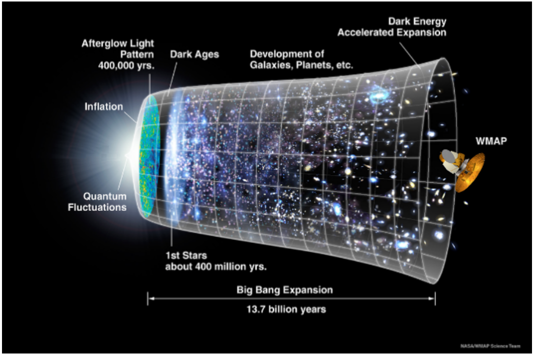

- For realistic cosmological models there are **certain conditions** that need to hold during the inflationary stage, for example we need to ensure:
  - a nearly scale invariant spectrum of perturbations ($n_s \simeq 1$)
  - a large enough number of e-folds N (generally of arround 50-60)

- One-field α-attractor models provide a very good fit to the latest observational results – almost independently of the choice of the inflaton potential they lead to an inflationary universe with **the right values** for $\mathbf{n_s}$ (the spectral index) and **r** (the tensor to scalar ratio).

- The most studied α-atractor models are the one-field models, but there are also multi-field models (based on the hyperbolic disk) that started to be studied, both theoretically and numerically.

- What makes these models more interesting is their geometric nature because observational predictions of these models are mostly determined by the **geometry of the scalar manifold** rather than the potential.

- The two-field α-attractor models arise from cosmological solutions of 4-dimensional gravity coupled to a nonlinear sigma model whose target space (scalar manifold) Σ is the Poincaré disk (the open unit disk endowed with its unique complete metric $\mathcal{G}$) of Gaussian curvature $K(\mathcal{G}) = -\frac{1}{3\alpha}$.

$$S[g,\varphi] = \int_X \mathrm{vol}_g \Big[-\frac{1}{2}\mathrm{R}(g) - \frac{1}{2}\mathrm{Tr}_g \varphi^*(\mathcal{G}) - V \circ \varphi \Big] \tag{1}$$

  - (X, g) is an oriented 4-dimensional Lorentzian manifold
  - $\mathrm{R}(g)$ is the scalar curvature of g
  - $\varphi : X \longrightarrow \Sigma$ is a smooth map which locally describes two real scalar fields
  - $\varphi^*(\mathcal{G})$ is the pull-back through φ of the metric $\mathcal{G}$
  - $V : \Sigma \to \mathbb{R}$ a smooth function (called the *scalar potential*)

Locally:

$$\mathrm{Tr}_g \varphi^*(\mathcal{G}) = g^{\mu\nu}\mathcal{G}_{\alpha\beta}\partial_\mu\varphi^\alpha\partial_\nu\varphi^\beta \quad , \quad \mu,\nu = 0,\ldots,3 \ , \quad \alpha,\beta = 1,2$$
$$(V \circ \varphi)(x^\mu) = V(\varphi^1(x^\mu), \varphi^2(x^\mu))$$

- Our generalized two-field α-attractor models are defined similarly, but with:
  - $(\Sigma, \mathcal{G})$ any oriented, connected, borderless and non-compact 2-dimensional Riemannian manifold with $K(\mathcal{G}) = -\frac{1}{3\alpha}$.

Definition

The *generalized two-field α-attractor model* is defined by the triplet $(\Sigma, \mathcal{G}, V)$, where $(\Sigma, \mathcal{G})$ is a complete hyperbolic surface with $K(\mathcal{G}) = -\frac{1}{3\alpha}$ for $\alpha > 0$, while $V : \Sigma \to \mathbb{R}$ is a smooth potential function

Let:

- $X = \mathbb{R}^4$ with global coordinates (t, x^1, x^2, x^3)
- $\mathrm{d}s^2 = -\mathrm{d}t^2 + a(t)^2 \sum_{i=1}^3 (\mathrm{d}x^i)^2$ (FLRW metric)
- $\varphi = \varphi(t)$ (independent of x^i)

The equations of motion reduce to:

$$\ddot{\varphi} + 3H\dot{\varphi} + \partial_\varphi V = 0 \tag{2}$$

$$\dot{H} + 3H^2 - V(\varphi) = 0 \tag{3}$$

$$\dot{H} + \frac{\dot{\varphi}^2}{2} = 0 \tag{4}$$

where $\dot{} = \frac{\mathrm{d}}{\mathrm{d}t}$ and:

$$H \stackrel{\mathrm{def.}}{=} \frac{\dot{a}}{a}$$

Assuming $H(t) > 0$, from (3) and (4) we get:

$$H(t) = \frac{1}{\sqrt{6}}\sqrt{\dot{\varphi}(t)^2 + 2V(\varphi(t))} \tag{5}$$

The first **slow roll** parameter:

$$\epsilon(t) \stackrel{\text{def.}}{=} -\frac{\dot{H}}{H^2} \quad ,$$

The conditions for inflation ($\dot{a} > 0$ and $\ddot{a} > 0$) are equivalent with:

$$0 < \epsilon(t) < 1$$

which together with the e.o.m. imply:

$$H(t) < \sqrt{\frac{V(\varphi(t))}{2}} \equiv H_c(\varphi(t)) \tag{6}$$

which gives the so-called inflationary regions of a trajectory $\varphi(t)$

Using (3), (5) and (6) gives that inflation happens when $\dot{\varphi}(t)^2 < V(\varphi(t))$.

A hyperbolic surface is a Riemannian surface, possibly non-compact, with complete Riemannian metric G having Gaussian curvature $K(G) = -1$.

Simple non-compact examples:

Poincaré half-plane $(\mathbb{H}, \mathrm{d}s^2_{\mathbb{H}})$ & Poincaré disk $(\mathbb{D}, \mathrm{d}s^2_{\mathbb{D}})$

(isometric with each other)

The Poincaré half-plane is the upper half-plane $\mathbb{H} \overset{\mathrm{def.}}{=} \{\tau \in \mathbb{C} | \ \mathrm{Im}\tau > 0\}$ endowed with its unique hyperbolic metric:

$$\mathrm{d}s^2_{\mathbb{H}} = \lambda^2_{\mathbb{H}}(\tau, \bar{\tau})\mathrm{d}\tau^2 \quad \text{with} \quad \lambda_{\mathbb{H}}(\tau, \bar{\tau}) = \frac{1}{\mathrm{Im}\tau} \quad .$$

The group of orientation-preserving isometries of $\mathbb{H}$ is $\mathrm{PSL}(2, \mathbb{R})$, acting on $\mathbb{H}$ through the Möbius transformation:

$$\tau \longrightarrow A\tau = \frac{a\tau + b}{c\tau + d}$$

The uniformization theorem (Poincaré - Koebe)

For any hyperbolic surface $(\Sigma, \mathcal{G})$ there is a surface group Γ and a locally isometric covering map (uniformization map) $\pi_{\mathbb{H}} : \mathbb{H} \longrightarrow \Sigma$ such that $\Sigma \simeq \mathbb{H}/\Gamma$.

A surface group is a discrete subgroup Γ of $\mathrm{PSL}(2, \mathbb{R})$ without elliptic elements (no $A \in \Gamma$ for which $|\mathrm{tr}(A)| < 2$).

How to use this theorem

To study the cosmological trajectories $\varphi(t) : X \longrightarrow \Sigma$ on the hyperbolic surface $(\Sigma, \mathcal{G})$ it is convenient to first study their lifted trajectories $\tilde{\varphi}(t)$ to $\mathbb{H}$

$$\tilde{\varphi}(t) : X \longrightarrow \mathbb{H}$$

and then to project them back to Σ

$$\varphi(t) = \pi_{\mathbb{H}} \circ \tilde{\varphi}(t)$$

Projecting back to Σ

The projection from $\mathbb{H}$ to Σ can be computed **only if** we know the uniformization map $\pi_{\mathbb{H}}$ explicitly or if we know the tiling of $\mathbb{H}$ determined by a fundamental polygon of Γ.

Cosmological applications of these models generally require sophisticated results from uniformization theory. For the special case of modular surfaces, those results are closely connected to number theory.

Note: We don't view the lifted model as being physical, but just as a tool for studying the original generalized α-atractor model defined by cosmological solutions of the e.o.m.

Computing fundamental polygons

There is no fully general algorithm known for computing fundamental polygons of surface groups. But a general algorithm is known for the case when Γ is an arithmetic Fuchsian group such that $\mathbb{H}/\Gamma$ has finite hyperbolic area.

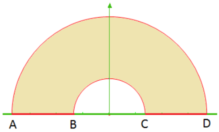

Figure: A fundamental polygon on $\mathbb{H}$ (for the group Γ generated by $\tau \to e^{l}\tau$)

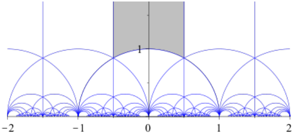

Figure: A fundamental polygon on $\mathbb{H}$ (for the modular group $\Gamma(2)$)

There are 4 types of ends: cusp ends, **flaring** (plane, horn and funnel) ends.

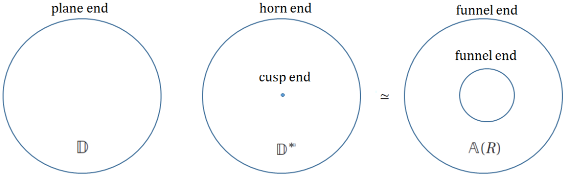

Figure: The elementary hyperbolic surfaces and the hyperbolic type of their ends.

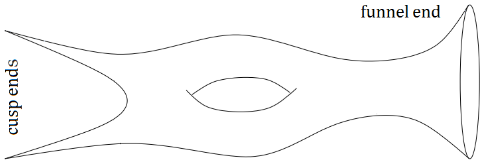

Figure: A non-elementary hyperbolic surface.

Let Σ be homeomorphic with $\hat{\Sigma} \setminus \{p_1, \dots, p_n\}$, where $\hat{\Sigma}$ is a borderless compact oriented surface and $p_1, \dots, p_n$ are a finite number of distinct points . $\hat{\Sigma}$ can be identified with the end compactification of Σ.

The conformal compactification $\bar{\Sigma}$ of Σ (taken with respect to a complex structure J on Σ) is the surface obtained by taking the closure of Σ inside $\hat{\Sigma}$.

We call conformal boundary the topological boundary $\partial_\infty \Sigma = \bar{\Sigma} \setminus \Sigma$. It consists of n_c isolated points and n_f disjoint closed curves, where $n_c + n_f = n$.

These two compactifications are conceptually important for understanding the behavior of our models near the ends of Σ.

(Examples: The end compactification of all elementary surfaces is S^2, while for the non-elementary surface on the previous page the end compactification is T^2.)

Let $\hat{\Sigma}$ be the end compactification of Σ.

A scalar potential $V : \Sigma \to \mathbb{R}$ is called well-behaved at an end $p \in \hat{\Sigma} \setminus \Sigma$ if there exists a smooth function $\hat{V}_p : \Sigma \sqcup \{p\} \to \mathbb{R}$ such that $V = \hat{V}_p|_\Sigma$.

The potential V is called globally well-behaved if there exists a globally-defined smooth function $\hat{V} : \hat{\Sigma} \to \mathbb{R}$ such that $V = \hat{V}|_\Sigma$. Thus V is globally well-behaved if it is well-behaved at each end of Σ.

We shall concentrate on **geometrically finite** hyperbolic surfaces.

Geometric finiteness

Let $(\Sigma, \mathcal{G})$ be a hyperbolic surface uniformized by the surface group $\Gamma \subset \mathrm{PSL}(2, \mathbb{R})$. One says that Γ and $(\Sigma, \mathcal{G})$ are geometrically finite iff any of the following equivalent statements holds:

- Γ admits a fundamental polygon with a finite number of sides.
- Γ (which is isomorphic with $\pi_1(\Sigma)$) is finitely-generated.
- $\Sigma \simeq \mathbb{H}/\Gamma$ is topologically finite (i.e. Σ has finite Euler characteristic $\chi(\Sigma) = 2 - 2\mathbf{g} - 2n$, where $\mathbf{g} =$ genus, $n =$ number of ends).

In particular, all elementary surfaces (i.e. the Poincare disk, hyperbolic punctured disk and the hyperbolic annuli) are geometrically finite.

In semi-geodesic coordinates in the neighborhood of an end $p \in \hat{\Sigma} \setminus \Sigma$, the hyperbolic metric can be brought to the following explicit form:

$$\mathrm{d}s_{\mathcal{G}}^2 \approx 3\alpha \left[\mathrm{d}r^2 + \left(\frac{C_p}{4\pi}\right)^2 e^{2\epsilon_p r}\mathrm{d}\theta^2\right]$$

where C_p and ϵ_p are known constants depending on the type of end (cusp, funnel, plane or horn), so the e.o.m. in a vicinity of an end reduce to:

$$\ddot{r} - 3\epsilon\alpha \left(\frac{C_p}{4\pi}\right)^2 e^{2\epsilon_p r}\dot{\theta}^2 + 3H\dot{r} + \frac{1}{3\alpha}\partial_r V = 0 \tag{7}$$

$$\ddot{\theta} + 2\epsilon_p \dot{r}\dot{\theta} + 3H\dot{\theta} + \frac{1}{3\alpha}\left(\frac{4\pi}{C_p}\right)^2 e^{-2\epsilon_p r}\partial_\theta V = 0 \tag{8}$$

The generic solution of this system has $\dot{r} \neq 0$ and $\dot{\theta} \neq 0$, thus being a portion of a spiral which "winds" around the ideal point.

Spiral trajectories near the ends

Since θ is periodic, a generic trajectory will spiral around the ends for any V well-behaved at the ends.

Inflation near the ends in the naive one-field truncation

Suppose that V is independent of θ in semigeodesic coordinates (r,θ) near some end and that it has an asymptotic expansion:

$$V(r)|_{r\gg 1} = V_0\left(1 - c\, e^{-r} + O(e^{-2r})\right)$$

where $V_0 > 0,\;\; c > 0$.

Then the generalized α-attractor model admits a local **naive** truncation to a one-field model, obtained by setting $\theta = \text{constant}$.

Universal behavior near the ends

Lazaroiu & Shahbazi showed that: for a well-behaved scalar potential near the ends, in the slow-roll approximation ($\epsilon \ll 1$) in the **naive** one-field truncation near the ends, all generalized two-filed α-attractor models lead to the same values of $\mathbf{n_s}$ and $\mathbf{r}$:

$$\mathbf{n_s} \approx 1 - \frac{2}{N}, \quad \mathbf{r} \approx \frac{12}{N^2} \;\; \text{(fitting the observational data)}$$

where $N \stackrel{\text{def.}}{=} \int_{t_0}^{t_f} H(t)\mathrm{d}t$ is the number of e-folds.

Examples:models based on certain planar surfaces

For a planar surface, the end compactification is the 2-sphere S^2. We considered the following examples of planar surfaces:

- The elementary hyperbolic surfaces: the hyperbolic disk (already studied before), the **hyperbolic punctured disk** and the **hyperbolic annuli**.
- The **hyperbolic triply-punctured sphere(=the modular curve** $Y(2)$**)**.

We choose certain scalar potentials V which are well-behaved on $\hat{\Sigma} = \mathrm{S}^2$, and which have the following simple forms on $\hat{\Sigma}$ in spherical coordinates:

$$\hat{V}_0(\psi, \theta) = 1 + \sin\psi\cos\theta \quad (9)$$

$$\hat{V}_+(\psi) = \cos^2\left(\frac{\psi}{2}\right) \quad (10)$$

$$\hat{V}_-(\psi) = \sin^2\left(\frac{\psi}{2}\right) \quad (11)$$

We analize examples of trajectories for Σ being $\mathbb{D}^*$, $\mathbb{A}(\mathbb{R})$ and $Y(2)$ for some chosen initial conditions and for a fixed $\alpha = \frac{1}{3}$.

Example 1: the hyperbolic punctured disk $\mathbb{D}^*$

The hyperbolic punctured disk is the punctured unit disk endowed with the unique complete hyperbolic metric:

$$\mathrm{d}s^2 = \lambda^2_{\mathbb{D}^*}(u,\bar{u})|\mathrm{d}u|^2 \ \ , \text{ where } \ \lambda_{\mathbb{D}^*}(u,\bar{u}) = \frac{1}{|u|\log(1/|u|)} \ \ (0<|u|<1) \ \ .$$

Here we have: $\Gamma \simeq \mathbb{Z}$, the holomorphic covering map $\pi_{\mathbb{H}} : \mathbb{H} \to \mathbb{D}^*$ is given by $\pi_{\mathbb{H}}(\tau) = e^{2\pi \mathbf{i} \tau}$, a fundamental polygon is $\mathcal{D}_{\mathbb{H}} = \{\tau \in \mathbb{H} \mid 0 \leq \mathrm{Re}(\tau) < 1\}$.

Choosing the globally well-behaved potential $\hat{V}_0$ given in (9), it takes the following form in polar coordinates on $\mathbb{D}^*$:

$$V_0 = 1 + \frac{2|\log\rho|}{1+(\log\rho)^2}\cos\theta \qquad (u = \rho e^{\mathbf{i}\theta})$$

and lifts to $\mathbb{H}$ as:

$$\tilde{V}_0 = V_0 \circ \pi_{\mathbb{H}} = 1 + \frac{4\pi y \cos(2\pi x)}{1+4\pi^2 y^2}$$

(since $u = \pi_{\mathbb{H}}(\tau) = e^{2\pi\mathbf{i}\tau}$ and $\tau = x + \mathbf{i}y$)

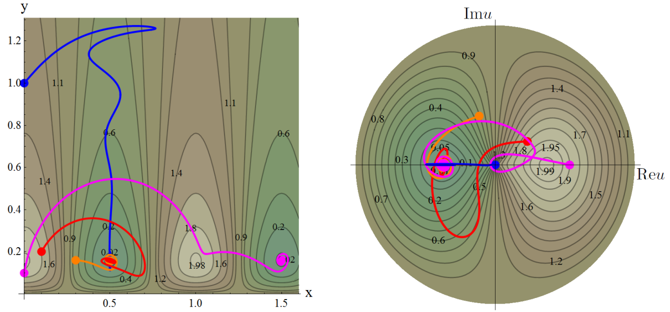

Figure: Trajectories $\tilde{\varphi}(t)$ on $\mathbb{H}$ and $\varphi(t)$ on $\mathbb{D}^*$ for the potential $\hat{V}_0$ and some chosen initial conditions $\tau_0 = x_0 + \mathbf{i}y_0$ and $\tilde{v}_0 = \tilde{v}_{0x} + \mathbf{i}\tilde{v}_{0y}$

trajectory	τ_0	$\tilde{v}_0$
orange	$0.3 + \mathbf{i}/(2\pi)$	0
red	$(1 + 2\mathbf{i})/10$	$2 + 3\mathbf{i}$
blue	$\mathbf{i}$	$1 + \mathbf{i}$
magenta	$\mathbf{i}/10$	$1.3 + 7\mathbf{i}$

Table 1. Initial conditions $\tau_0 = x_0 + \mathbf{i}y_0$ and $\tilde{v}_0 = \tilde{v}_{0x} + \mathbf{i}\tilde{v}_{0y}$.

For the well-behaved potential $\hat{V}_+$, we have: $V_+ = \frac{1}{1+(\log\rho)^2}$, $\tilde{V}_+ = \frac{1}{1+(2\pi y)^2}$.

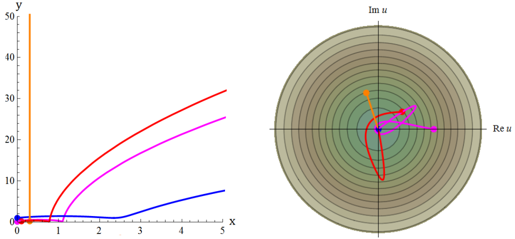

Figure: Trajectories for the potential $\hat{V}_+$ on $\mathbb{H}$ and $\mathbb{D}^*$ in the same initial condition

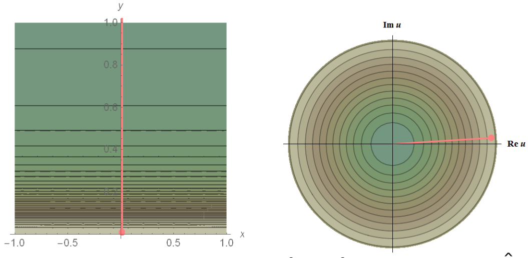

Figure: Example of trajectory with N=55.5 e-folds for the potential $\hat{V}_+$ on $\mathbb{H}$ and $\mathbb{D}^*$.
Iinitial conditions $\tau_0 = 0.001 + 0.0009\mathbf{i}$, $\tilde{v}_0 = 0$.

The annulus:

$$\mathbb{A}(R) = \{u \in \mathbb{C} \mid \frac{1}{R} \leq |u| \leq R\} \quad (R > 1)$$

has the unique complete hyperbolic metric:

$$\mathrm{d}s^2 = |\lambda_R(u)|^2 |\mathrm{d}u|^2 \quad , \text{ where } \quad \lambda_R(u) = \frac{\pi}{2\log R} \frac{1}{|u| \cos\left(\frac{\pi \log |u|}{2 \log R}\right)} \quad .$$

It is uniformized to $\mathbb{H}$ by the group Γ generated by $\tau \to e^{\ell}\tau$, where $\ell = \frac{\pi^2}{\log R}$.

The potential $\hat{V}_0$ takes the following form on $\mathbb{A}(R)$:

$$V_0 = 1 + \frac{2 \log \frac{R - \frac{1}{R}}{\rho - \frac{1}{R}}}{1 + \left(\log \frac{R - \frac{1}{R}}{\rho - \frac{1}{R}}\right)^2} \cos\theta$$

and lifts to $\mathbb{H}$ as:

$$\tilde{V}_0(\tau) = 1 + \frac{2 \log \frac{R - \frac{1}{R}}{\rho(\tau) - \frac{1}{R}}}{1 + \left(\log \frac{R - \frac{1}{R}}{\rho(\tau) - \frac{1}{R}}\right)^2} \cos\left(\frac{2\pi}{\ell} \log|\tau|\right)$$

where $\rho(\tau) = e^{\frac{\pi^2}{\ell} - \frac{4\pi^2}{\ell^2} \log|\tau|}$

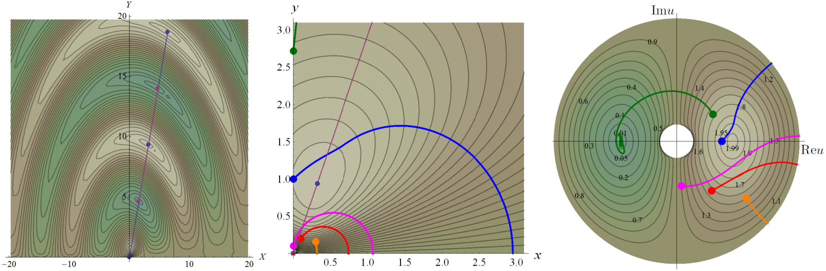

Figure: Examples of trajectories for the potential $\hat{V}_0$ on $\mathbb{H}$ and $\mathbb{A}(R)$. The initial conditions are as in Table 1, plus those for the green trajectory: $\tau_0 = \mathbf{i}e$, $\tilde{v}_0 = 1 + 10\mathbf{i}$.

Choices of trajectories on $\mathbb{H}$ and $\mathbb{A}(R)$

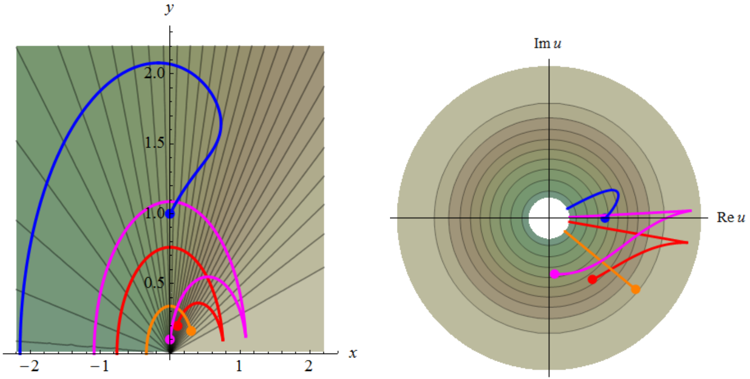

Figure: Examples of trajectories for the potential $\hat{V}_+$ on $\mathbb{H}$ and $\mathbb{A}(R)$ and the initial conditions in Table 1.

The triply punctured sphere $\Sigma = Y(2) \stackrel{\mathrm{def.}}{=} \mathbb{CP}^1 \setminus \{p_1, p_2, p_3\}$ endowed with the hyperbolic metric:

$$\mathrm{d}s^2 = \rho(\zeta,\bar\zeta)^2 \mathrm{d}\zeta^2 \ ,$$

where:

$$\rho(\zeta,\bar\zeta) = \frac{\pi}{8|\zeta(1-\zeta)|}\frac{1}{\mathrm{Re}[\mathcal{K}(\zeta)\mathcal{K}(1-\bar\zeta)]} \ , \quad \mathcal{K}(\zeta) = \int_0^1 \frac{\mathrm{d}t}{\sqrt{(1-t^2)(1-\zeta t^2)}}$$

Y(2)

Each of the three punctures corresponds to a cusp end.
Its end compactification is $\hat\Sigma = \mathrm{S}^2$.
It is conformal to $\mathbb{C} \setminus \{0, 1\}$.

$Y(2)$ is uniformized by the principal congruence subgroup of level 2:

$$\Gamma(2) \stackrel{\text{def.}}{=} \left\{ A = \left[\begin{array}{cc} a & b \\ c & d \end{array} \right] \in \mathrm{PSL}(2, \mathbb{Z}) \mid a, d = \mathrm{odd} \ , \ b, c = \mathrm{even} \right\}$$

with uniformization map $\pi_{\mathbb{H}} : \mathbb{H} \to Y(2)$ given by the elliptic modular lambda function:

$$\pi_H(\tau) \equiv \lambda(\tau) = \frac{\wp_\tau\left(\frac{1+\tau}{2}\right) - \wp_\tau\left(\frac{\tau}{2}\right)}{\wp_\tau\left(\frac{1}{2}\right) - \wp_\tau\left(\frac{\tau}{2}\right)}$$

where $\wp$ is the Weierstrass elliptic function of modulus τ.

trajectory	τ_0	$\tilde{v}_0$
black	$0.4 + 0.5\mathbf{i}$	$0.3 + \mathbf{i}$
red	$1.4 + 0.5\mathbf{i}$	$0.1 + 0.2\mathbf{i}$
magenta	$0.2 + 0.7\mathbf{i}$	$0.7 + 0.5\mathbf{i}$
yellow	$0.3 + 0.5\mathbf{i}$	0
orange	$0.99 + 0.415\mathbf{i}$	0

Table 2. Initial conditions $\tau_0 = x_0 + \mathbf{i}y_0$ and $\tilde{v}_0 = \tilde{v}_{0x} + \mathbf{i}\tilde{v}_{0y}$ on $\mathbb{H}$

For the potential $\hat{V}_+$ we have:

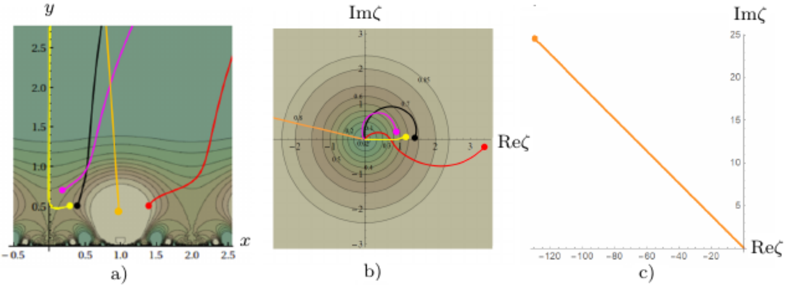

Figure: a) Level plots of the lifted potential $\tilde{V}_+$ on $\mathbb{H}$ and some lifted trajectories with initial conditions given in Table 2. b) Level plots of V_+ on $\mathbb{C} \setminus \{0, 1\}$ and the corresponding projected trajectories. c) The full orange trajectory on $\mathbb{C} \setminus \{0, 1\}$.

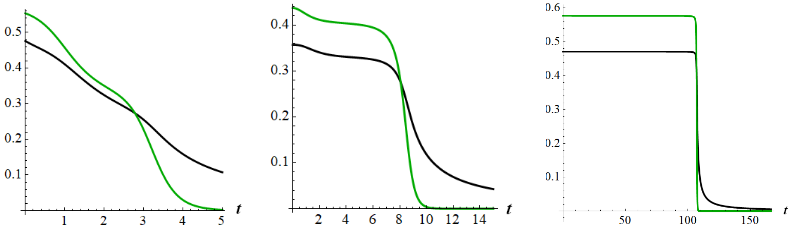

Figure: Plot of $H(t)$ (black) and $H_c(t)$ (green) for the red, yellow and orange trajectories in the potential $\tilde{V}_+$. The red and yellow trajectorie have small number of e-folds (less than 2), but the orange trajectory has 50 e-folds.

For the same initial conditions as in Table 2, but for the scalar potential $\hat{V}_0$

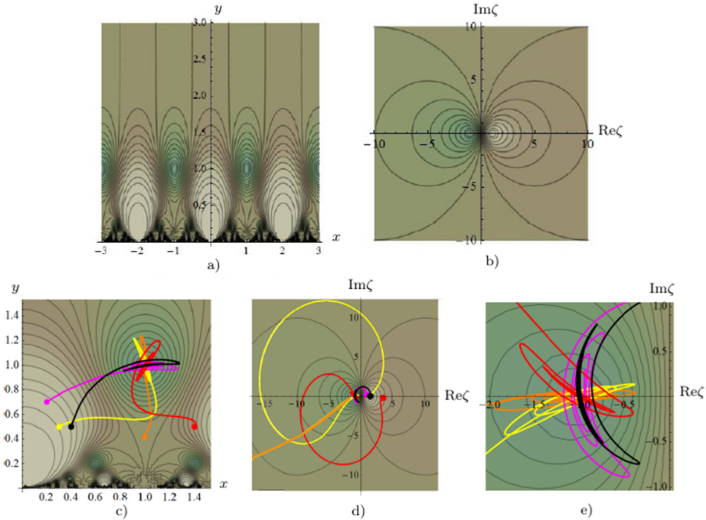

Figure: Level plof of $\tilde{V}_0$ on $\mathbb{H}$ and V_0 on $Y(2)$. Trajectories on $\mathbb{H}$ and $\mathbb{C} \setminus \{0, 1\}$.

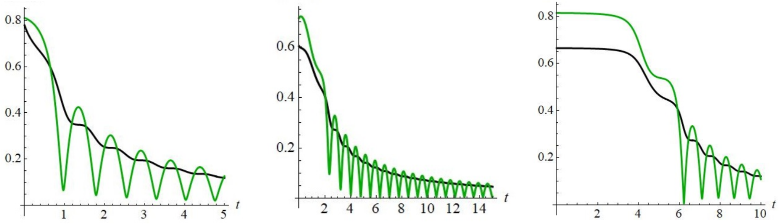

Figure: Plot of $H(t)$ (black) and $H_c(t)$ (green) for the magenta and red and yellow trajectories in $\tilde{V}_0$.

Trajectory with $N = 56$ efolds in potential $\tilde{V}_-$

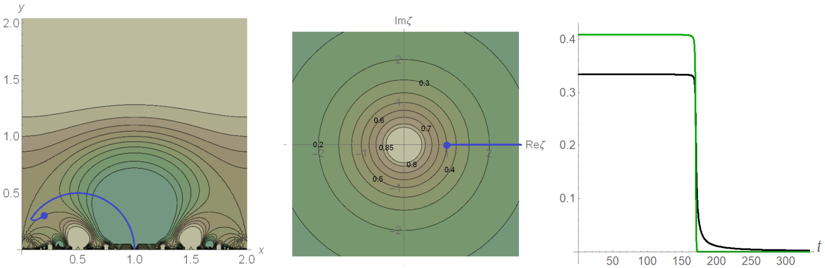

Figure: Trajectory on $\mathbb{H}$ and $\mathbb{C} \setminus \{0, 1\}$ with initial conditions on $\mathbb{H}$: $\tau_0 = 0.198 + 0.3\mathbf{i}$ and $\tilde{v}_0 = 0$. Plot of $H(t)$ (black) and $H_c(t)$ (green) for this blue trajectory.

Conclusions:

- We proposed a wide generalization of two-field α-attractor models obtained by promoting the scalar manifold from the Poincaré disk to a **general geometrically-finite non-compact hyperbolic surface**.
- Our generalized models are parameterized by a positive constant α, by the choice of a surface group $\Gamma \in \mathrm{PSL}(2, \mathbb{R})$ and by the choice of a smooth well-behaved scalar potential V.
- We proposed a general procedure for studying such models through **uniformization techniques** and **without using one-field truncations**.
- We showed that such models have the same universal behavior as ordinary α-attractors in a naive one-field truncation near each end, provided that the scalar potential is well-behaved near that end.

On-going work (with L. Anguelova & C. I. Lazaroiu):

- finding more realistic potentials and trajectories, compatible with the observational data and satisfying Noether symmetries.

This talk was based on the following papers:

- E. M. Babalic, C. I. Lazaroiu, *Generalized α-attractor models from elementary hyperbolic surfaces*, Adv. Math. Phys., Vol. 2018, ID 7323090 [arXiv:1703.01650].
- E. M. Babalic, C. I. Lazaroiu, *Generalized α-attractors from the hyperbolic triply-punctured sphere*, arXiv:1703.06033.
- C. I. Lazaroiu, C. S. Shahbazi *Generalized α-attractor models from geometrically finite hyperbolic surfaces*, arXiv:1702.06484.